Digest Journal of Nanomaterials and Biostructures Vol. 7, No. 4, October-December 2012, p. 1667-1677

CORTICAL BONE AS RESOURCE FOR PRODUCING BIOMIMETIC MATERIALS FOR CLINICAL USE

F. MICULESCU[a,*], G. E. STAN[b], L. T. CIOCAN[c], M. MICULESCU[a], A. BERBECARU[a], I. ANTONIAC[a]
[a]*Politehnica University of Bucharest, Faculty of Materials Science and Engineering, Bucharest 060042, Romania*
[b]*National Institute of Materials Physics, P.O. Box MG-7, Bucharest-Magurele 077125, Romania*
[c]*"Carol Davila" University of Medicine and Pharmacy, Bucharest 020022, Romania*

The search of new alternative materials for bone reconstruction is a major objective in biomaterials engineering and reconstructive medicine. In this study the compact bone derived materials are proposed, their structure and composition being modified by thermal treatments performed in 200–1200°C range, using 200°C temperature steps. The monitoring of the bone modifications under heat-treatment was carried out using thermal analysis (TGA-DSC), microstructural (SEM), compositional (EDS) and structural (FTIR, XRD) methods. Tailoring the bone material's morphological, chemical and structural properties by heat-treatments, expressed by the HA/β-TCP compositional ratio, degree of crystallinity and porosity control, could lead to the obtaining of good quality bone substitute materials suitable for the bone regeneration of large osseous defects.

(Received August 15, 2012; Accepted October 25, 2012)

Keywords: Bone graft, Calcium phosphate, Hydroxyapatite, microstructure

1. Introduction

The conjunctive hard tissue (bone) is characterized by composition, crystalline structure, crystallite size, morphology and orientation. Many studies have reported important differences in terms of solubility between the biological and synthetic apatite materials [1-3]. The small crystallite size combined with nonstoichiometric composition, internal crystal disorder and the presence of carbonate ions and other impurities in their structure, explain the particular behaviour of biological apatites [2,4-8]. The possibility of using the cortical or trabecular bone taken from the patient or from donors (extracted by invasive techniques but without affecting any natural functions), was studied frantically [9]. The autologous bone (*autografts*) is considered the performance standard in terms of biocompatibility. However the autografts have significant limitations, such as the donor's morbidity, tissue rejection and inappropriate tissue shape. There is also a growing interest in alternative bone grafts, concerning the tissue transplantation from one individual to another of the same species with a different genotype (*allograft*). Although attractive, the allografts imply also some drawbacks as the disease transmission, immunogenicity, patient risk, and the high surgical costs. In this context, many efforts have been made to develop ideal products for bone grafts substitutes and scaffolds [10-12]. The study of animal bones is a major objective of the biomaterials engineering and reconstructive medicine fields, as this type of natural-biological biomaterial could constitute a low cost and accessible resource, offering, also, excellent medical results, when used in the optimal conditions [4,5, 12-15]. The positive effects on bone formation of the biphasic calcium phosphate (BCP) bioceramics (hydroxyapatite [HA,

*Corresponding author: f_miculescu@yahoo.com

$Ca_{10}(PO_4)_6(OH)_2$] and β-tricalcium phosphate [β-TCP, $Ca_3(PO_4)_2$] mixtures) and the superiority to HA in terms of bone formation speed has been demonstrated [16-19].

In this study, we aim to obtain improved bulk materials for major defects' reconstruction from human compact bone pieces (sampled by resection of the femoral head and part of the upper femur) by performing thermal treatments at certain temperatures. The thermal treatments were used to eliminate the hazard of any potentially transmitted diseases and to obtain various BCP HA/ β-TCP ratios and crystallinity degrees which in turn control the *in vivo* resorbability. Thermal analysis (TGA-DSC) microstructural (SEM), compositional (EDS) and structural (XRD, FTIR) analyses were performed on the samples, in order to highlight the best characteristics for their potential use in reconstruction surgery (bone graft and scaffolds), as alternative to traditional products, such as synthetic HA and β-TCP. In the same time, we aimed to emphasize the microstructural changes and interactions between mineral phase and the organic one that occurs during heat-treatments. The study will indicate how powder and compact products, which may be used as primary scaffolds for the reconstruction and remodelling of morphological osseous defects, could be successfully fabricated using cheap source materials and technological processes.

2. Experimental

2.1 *Samples' preparation*

The samples preparation was performed in the laboratories of the University Politehnica from Bucharest, Materials Science and Engineering Department. The materials used to perform the experiments were collected from the human femoral head and femoral compact bone, being frozen immediately after sampling.. All the femoral bones were placed in individual containers. The preparation of a biomaterial of biological origin, for possible applications in bone reconstruction, involved, in a first step, the removal of hazardous organic components in order to avoid any immunological and antigenic contamination. For the removal of the blood, proteins, macroscopic impurities and adhered substances (including salts, ligaments and tissues stuck to the bone), the samples were cleaned with surgical blades and forceps, and subsequently treated in jet of hot water, steam (at 100°C and 1 atm) and solvents. The cortical bone samples were dried by placing them in desiccators and cutting them into square pieces (5 mm x 5 mm x 5 mm) using a jig saw with diamond blade. The heat-treatments (HT) were carried out in a controlled atmosphere furnace (Ar) at 200°C, 400°C, 600°C, 800°C, 1000°C, and 1200°C for 12 hours. The selected upper limit temperature was 1200°C, whereas above this value β-TCP to α-TCP phase transition is known to occur [5,20].

2.2 Characterization techniques

The TGA-DSC analysis was performed with a *SDT Q600* instrument, in a 25–1250°C temperature range, using a 10°C/min heating rate. Throughout the analysis, the instrument sample chamber has been purged with 20 ml/min Ar flow rate.

For analysis by SEM microscopy and EDS microanalysis the samples were examined in a *Philips XL 30 ESEM TMP* scanning electron microscope, equipped with an auxiliary microanalysis EDS system (*EDAX Sapphire UTW*, 128 eV resolution). The EDS method involved qualitative and quantitative microanalysis. The microscopy and/or microanalysis operating conditions were as follows: 0° tilt angle, 35° take of angle, 25 kV accelerating voltage, and 10 mm working distance. Due to special performance of the apparatus no conductive coating was necessary for these analyses.

Fourier transform infrared (FTIR) spectroscopy was used for analyzing the functional groups present in the samples. The analyses were performed with a *Perkin Elmer BX Spectrum* spectrometer, in attenuated total reflection mode (ATR) using a *Pike-MIRacle* diamond head of 1.8 mm diameter. The spectra were recorded in the range 4000–400 cm^{-1}, at a resolution of 4 cm^{-1}, with a total of 100 scans per experiment.

The crystallographic structure of each sample was analyzed by X-ray diffraction (XRD) on a *Pananalytical* diffractometer, equipped with Cu target X-ray tube (λ = 1.5418 Å), and operated at 30 kV accelerating voltage, 25 mA current. The scattered intensity was scanned in the range 20–60° (2θ), with a step size of 0.02°, and 4 seconds per step.

3. Results

3.1 TGA-DSC results

TGA analysis (Figure 1) showed a decrease of weight during the heating up to 1250°C: from 10.236 mg at 25°C to 4.252 mg at the final temperature, which corresponds to a 41.54% total weight loss. The first significant weight loss was recorded at 250°C (1.668 mg) representing 16.3% of the total sample mass, and was associated to the massive dehydration of the sample [21].

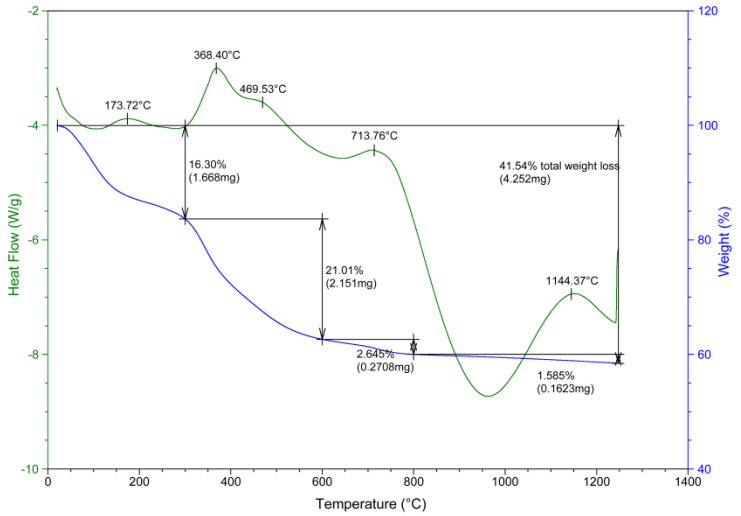

Fig. 1. Comparison of the TGA (right axis) and DSC (left axis) spectra obtained on the heat-treated bone samples.

The sample reduced its weight with 21.01% (2.1541 mg) when heated at 600°C, which can be associated with the collagen elimination from the bone structure. This reaction continues up to 800°C, at a lower rate, the weight difference registered between 600°C and 800°C temperatures being of only 2.645% (0.27 mg). Above this temperature, a fine descending slope is observed, at the maximum chosen temperature (1250°C) the weight loss being of 0.1623 mg (1.585%), associated with the removal of carbonized organic components and the incipient transformation of HA in β-TCP (as will be shown by EDS and XRD analysis).

DSC curve (also presented in Figure 1) proffered additional information about the structural changes and the temperatures at which they occur. The first detectable change has occurred in the 120–140°C range, having its maximum at 174°C. Above this temperature, at 310°C a transformation began, with the maximum at 370°C, which is completed at 415°C. At this temperature a new transformation started, which is finalized at 480°C, and has its maximum at 470°C. The next transformation had the maximum at 655°C being completed at 715°C. After this temperature, one can notice that the DSC slope dramatically decreased up to 925°C, a phase transformation being completed at 1000°C began, having a minimum at 960°C. Finally, in the last temperature interval, a major transformation began, and completed at 1245°C, having a maximum at 1145°C. These phenomena could be related to the physical transformation of the material determined by water and organic components elimination, the continuous increase of the mineral phase crystallinity with the temperature, and, in the end, to the partial transformation of HA into β-TCP. These changes will be confirmed by SEM-EDS, FTIR and XRD, and will be discussed in detail further.

3.2 SEM-EDS analysis

At a macroscopic level, progressive colour changes, delaminating, fracturing and distortion processes have been observed with the heat-treatment temperature. Significant morphological changes have also occurred at the microstructural level. Figure 2 presents the SEM images obtained in MIX signal, a morpho-compositional type analysis, in fact combination of the secondary (SE) and backscattered electrons (BSE) signals. At a higher magnification (5000x) collagen microfilaments can be distinguished. Similar organic filaments have been previously reported by other authors, this type of formations being discovered in micro-cracks of the cortical bone [22,23]. Normal bone, untreated, contains small pores, but overall raw bone microstructure is very dense due to the presence of organic matter associated to inorganic mineral-impregnated bone (Figure 2-a). After the bone was heated at 200°C (Figure 2-b) and 400°C (Figure 2-c) for 12 hours, the microstructure has changed as a result of the water and organic matter content (collagen, present in small amounts, and perhaps proteins, polysaccharides and lipids) elimination [5]. Figure 2-d reveals a layered architecture of mainly inorganic and remains of organic components resulting from the application of the 600°C heat-treatment. The sample microstructure clearly indicated that the components are interconnected [24-26]. In Figure 2-d–inset different aspects of the natural bone microstructure (containing water, proteins and collagen) can still be observed, compared to thermally treated bone at higher temperatures (from which the organic components were mostly removed). When increasing the temperature above 600°C (Figure 2-e) pores formation take place. The pores are different than the ones present in the untreated bone, their surfaces is rough and branched, and not preponderantly smooth. The heat-treatments at higher temperatures (Figure 2-e,f,g) lead to the appearance of apatite crystals, in agreement with other studies [22]. The degeneration of the organic matrix under the influence of temperature is known to have a great impact on the bone mechanical properties [27,28]. In healthy bone, the main degradation mechanism is delamination of the trabecular contour, while, in the bone with organic component removed by heat-treatment (Figure 2-f,g) the morphology becomes granular with large and interconnected pores [29,30]. For comparison reasons there are presented also the microstructures for two commercial products found nowadays in clinical use: hydroxyapatite (Figure 2-h) and β-tricalcium phosphate (Figure 2-i).

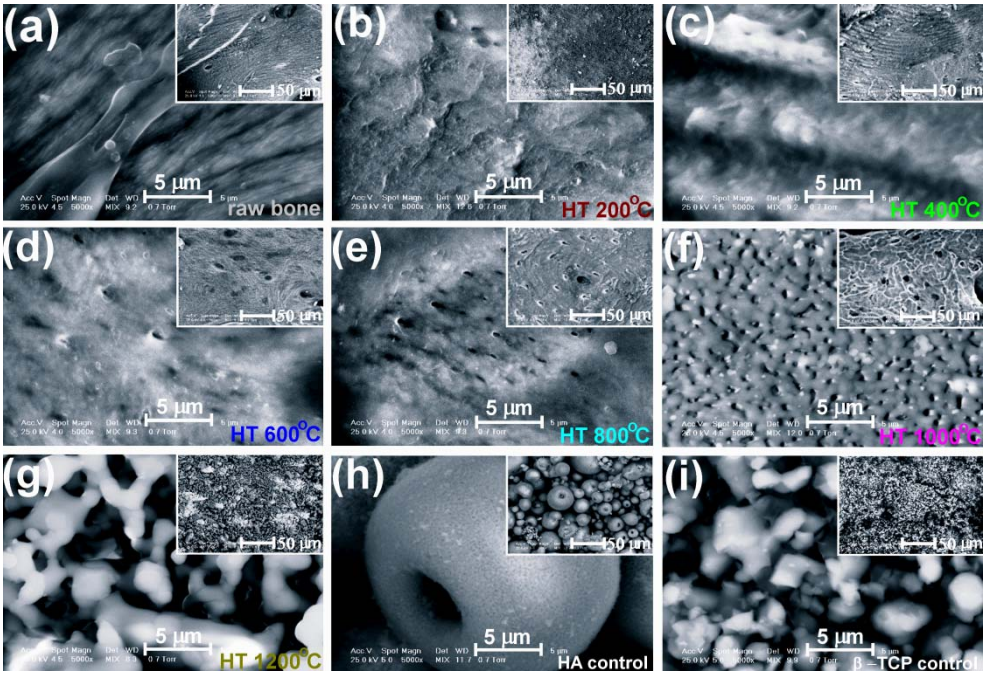

Fig. 2. Detailed view and panoramic view (inset) SEM images of the raw bone (a), sample heat-treated at 200°C (b), 400°C (c), 600°C (d), 800°C (e), 1000°C (f), 1200°C (g), as well as for the HA (h) and β-TCP (i) controls.

The EDS spectra of the standard samples and of bone-derived samples are presented comparatively in Figure 3. In the heat-treated bone samples the presence of other chemical elements besides Ca and P (such as Na, Mg, Si, O, C) was revealed, characteristic of a normal bone chemical composition (see Figure 3). One can notice that the heat-treatment temperature increase does not significantly influences the bone samples qualitative composition, except a remarkable decrease of the C concentration.

The quantitative EDS analyses provided us the Ca/P ratios for the studied bone samples (Table 1). In a first step, in order to assess the accuracy of the EDS results, elemental composition analyses were conducted on standard HA and β-TCP, revealing stoichiometric Ca/P molar ratio values, of 1.67 for HA and of 1.50 for β-TCP, and thus, asserting the accuracy of the method.

Table 1. Ca/P molar ratios values determined by EDS.

Raw bone	HT 200°C	HT 400°C	HT 600°C	HT 800°C	HT 1000°C	HT 1200°C	HA control	β-TCP control
1.69	1.66	1.63	1.54	1.53	1.51	1.48	1.67	1.50

The quantitative EDS data presented in Table 1 confirm, in relation with the XRD and FTIR results presented hereafter, that, although there are microstructural and crystallographic similarities with synthetic HA, the biological hard tissues apatites are non-stoichiometric, with microstructural imperfections caused by the incorporation in the crystalline network of various chemical elements in small quantities.

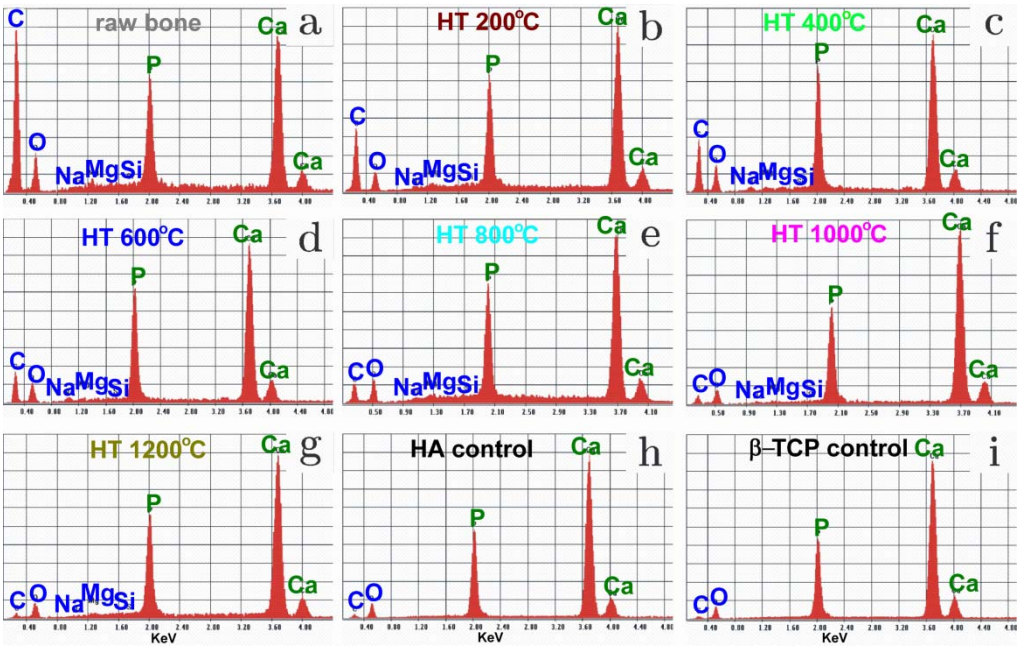

Fig. 3. Comparison of the EDS spectra obtained for the raw bone (a), sample heat-treated at 200°C (b), 400°C (c), 600°C (d), 800°C (e), 1000°C (f), 1200°C (g), as well as for the HA (h) and β-TCP (i) controls.

3.3 FTIR measurements

The FTIR spectra are represented in Figure 4. The vibrational modes assignation is summarized in Table 2. The FTIR spectrum of the raw bone displays a broad band in range of 2500–3700 cm^{-1} generated by ν_1 and ν_3 stretching modes of hydrogen-bonded H_2O molecules. The 2700–3100 cm^{-1} region is characteristic for C–H stretch vibrations from sp^3– and sp^2–hybridized CH_n, corresponding to the organic compounds present in bone. The band present at 2958 cm^{-1} could be attributed to asymmetric C-H bonds in the aliphatic chains of collagen, while the bands

positioned at 2918 cm^{-1} and 2877 cm^{-1} could correspond to the superimposing of sp^3 CH_2 asymmetric and sp^3 CH modes and to the sp^3 CH_3 symmetric vibration mode, respectively [31,32]. The three specific collagen amide absorption bands were also identified: amide I in 1600–1700 cm^{-1} range (C=O stretching vibrations), amide II in 1500–1550 cm^{-1} range (N-H deformation) and amide III in 1200–1300 cm^{-1} range (N-H deformation and other complex modes resulting from a mixture of several coordinate displacements). Usually, the amide I band is strong, the amide II band is weak and the amide III band is moderate [33]. One should also take into account the superimposed contribution in this spectral range of the O–H ν_2 bending mode (1641 cm^{-1}) [34]. The absorption bands positioned at lower wave numbers could be assigned to bending mode of PØP Q^3, Q^2, Q^1 and Q^0 units (550–610 cm^{-1}) and to symmetric stretching bands of PØP Q^3, Q^2 and Q^1 units (650–800 cm^{-1}), respectively. The weak band centred at ~960 cm^{-1} is attributed to the $(PO_4)^{3-}$ (ν_1) symmetric stretching mode, while the sharper and intenser bands in 1000–1200 cm^{-1} region correspond to the triple degenerated (ν_3) asymmetric stretching of phosphate groups (Table 2). One should note that the shoulder positioned at the higher wave number (~1160 cm^{-1}) could also shadow the presence of a low intensity acid phosphate band [34,35], more easily distinguishable by the well defined shoulder centred at 871 cm^{-1}.

The broad band, in 2500–3700 cm^{-1} range, assigned to H-O-H bonds, suggested that a large quantity of adsorbed water is present in the raw material (most probably in structural intervoids). The raw material is not only strongly hydroxylated, but also carbonated: sharp C–O asymmetric stretching (ν_3) lines at (~1410 and ~1455 cm^{-1}). Besides, the vibrational band positioned at ~871 cm^{-1} could be the result of the overlapping of the signature band of $(HPO_4)^{2-}$ with the $(CO_3)^{2-}$ (ν_2) bending mode. The position of the $(CO_3)^{2-}$ stretching bands denote a "B-type" carbonatation of the bone mineral (the replacement of $(PO_4)^{3-}$ ions in the HA lattice) [36]. The nature of the vibrational bands was elucidated by the successive annealings treatments performed at temperatures up to 1200°C.

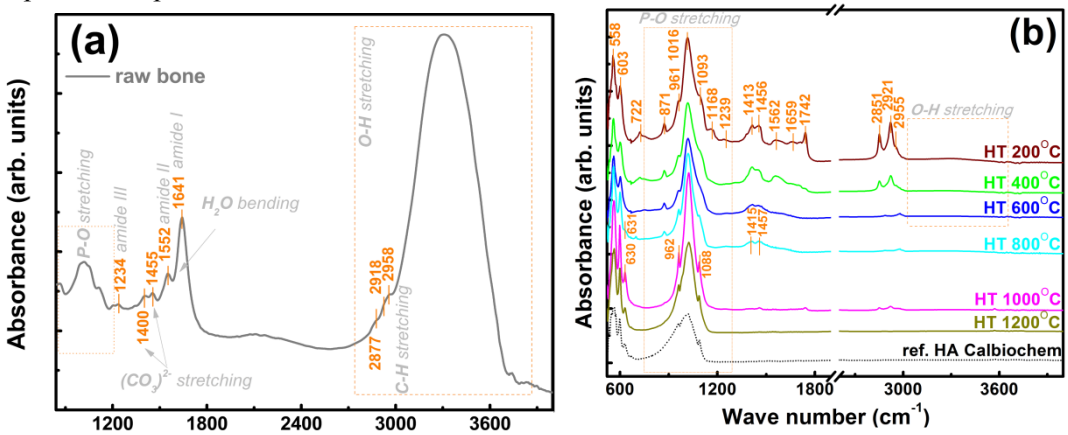

Fig. 4. FTIR spectra of raw bone (a) and heat-treated bone samples (b).

We observe a progressive decrease of water, CH_n and carbonate stretching bands' intensity with the annealing temperature. The IR bands of water are extinct at 400°C, in agreement with other results from literature [37]. The $(CO_3)^{2-}$ and CH_n bands areas are decreasing monotonously up to 400°C, and more dramatically up to 800°C, while at 1000°C and 1200°C these bands are no longer visible. Therefore, one can deduce that at annealing temperatures between 200 and 400°C, bone absorbed water and collagen structure bounded water is lost, the full dehydration being evidenced by the disappearance of the broad band attributed to hydrogen-bonded H_2O molecules (in 2500–3700 cm^{-1} range). After the annealing at 400°C the CH_n absorption bands ((in 2700–3100 cm^{-1} range) can still be seen, but as the temperature increases (up to 600°C) their intensity drastically decrease, indicating the beginning of collagen degradation (breaking the macromolecular aliphatic chains) [38]. The results are consistent with the TGA-DSC observations presented above. Moreover this result is in agreement with the EDS results which showed a continuous decrease of C content with temperature.

Table 2. Assignment of FTIR vibration bands for the raw bone and heat-treated samples.

VIBRATION BAND	SAMPLE			
	raw bone	HT 200-600°C	HT 800°C	HT 1000-1200°C
$(PO_4)^{3-}$ (ν_4) asymm. bending mode	556	558	558	558
$(PO_4)^{3-}$ (ν_4) asymm. bending mode	604	603	603	603
OH libration	–	–	631	630
PØP Q^3, Q^2 and Q^1 units symm. stretching	722	722	–	–
$(HPO_4)^{2-}$ ions vibrations $(CO_3)^{2-}$ (ν_2) asymm. bending mode	875	871	871	–
$(PO_4)^{3-}$ (ν_1) symm. stretching mode	965	960	962	962
$(PO_4)^{3-}$ (ν_3) asymm. stretching mode	1016–1097	1019–1083	1019–1093	1019–1093
$(HPO_4)^{2-}$ ions vibrations $(PO_4)^{3-}$ (ν_3) asymm. stretching mode	1180	1168	-	-
amide III vibrations	1234	1239*	-	-
$(CO_3)^{2-}$ (ν_3) asymm. stretching mode	1400	1413	1415	-
$(CO_3)^{2-}$ (ν_3) asymm. stretching mode	1455	1456	1457	-
amide II vibrations	1552	1562	-	-
amide I vibrations H-O-H (ν_2) bending mode	1641	1659,1742		-
sp^3– and sp^2–hybridized CH_n stretching vibrations	2958, 2918, 2877	2955,2921,2851	-	-
ν_1 and ν_3 stretching modes of hydrogen-bonded H_2O molecules	2500–3700	2500–3700*	-	-

**present only for 200°C heat-treated sample*

The $(PO_4)^{3-}$ IR bands of bone mineral phase shape modifies continuously, becoming more and more narrow. The phosphate bending and stretching bands became more conspicuous after 800°C. The sharpness of these bands along with the appearance of a new bad positioned at ~630 cm^{-1} (vibrational mode of structural OH) and the extinction of the $(HPO_4)^{2-}$ bands are an evidence of the expected increase of the short range order in the crystalline hydroxyapatite structure [37,39]. The decrease of phosphate stretching bands' overall area after the 1200°C heat-treatment suggest that structural transformations occurred in the bone mineral phase, which correlates well with the XRD findings presented hereafter.

3.3 XRD results

The XRD patterns (Figure 5) revealed a progressive crystallization of the sample with the increase of the heat-treatment temperature. The sample structure is predominantly amorphous up to 800°C, while at 1000°C crystallization is induced (ICDD: 9-432) with HA as a prominent phase, along β-TCP (ICDD: 55-0898), as a secondary phase, but whose intensity is increasing with the temperature (1200°C). This was to be expected, based on the EDS results (Figure 3, Table 1), as in the non-stoichiometric compositions, at high temperatures, HA is known to partially transform into tricalcium phosphate.

Interestingly, a secondary parasitic phase is observed at $2\theta \approx 26.6°$ in the raw bone sample, its intensity increased with the heat-treatment up to 800°C, disappearing at higher temperature. The identification based on a singular line is hard, however this phase could be associated to a SiO_2 quartz phase (ICDD: 81-0065) – determined by some impurities – or to a calcium hydrogen phosphate phase (ICDD: 70-6384).

Rietveld quantitative analysis has been performed using the MAUD v.2.31 software [40] for these later two patterns. After the 1000°C annealing, the sample consist of a BCP ceramic (HA + β-TCP), having a β-TCP content of ~20%. By increasing the heat-treatment temperature at 1200°C, the β-TCP phase weight increases to ~30%.

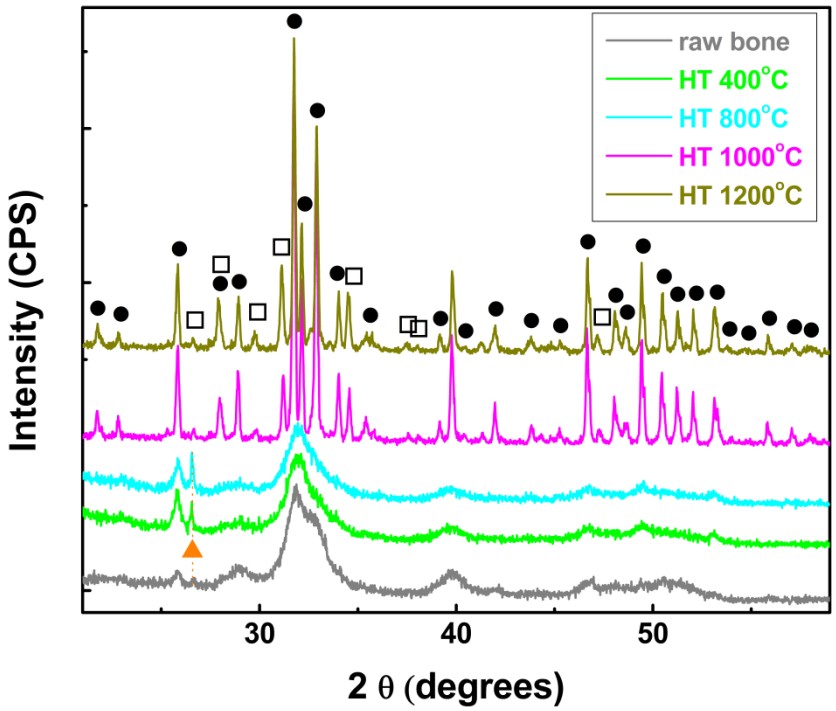

Fig. 5. XRD patterns of raw bone and heat-treated bone samples.● – hydroxyapatite; □ – calcium phosphate (whitlockite); ▲– quartz or calcium hydrogen phosphate phase

Table 3. HA/β-TCP ratios and HA lattice parameters for control and heat-treated samples.

Sample	HA control	HT 1000°C	HT 1200°C
Space group	Hexagonal, $P6_3/m$ (176)		
Lattice parameter, *a* (Å)	9.418	9.421	9.416
Lattice parameter, *c* (Å)	6.884	6.886	6.888
HA : β-TCP	100 : 0	80.5 : 19.5	69.2 : 30.8

The HA cell parameters also present slight variations with the increasing annealing temperature (Table 3), this being an indicative of structural modifications associated with the removal of soluble CO_2 from the B-type HA structure at higher temperatures. The possibility for a small fraction of the soluble CO_2 to chemically react forming calcium carbonate, leading to a chemical composition modification of the apatite material, should be taken into account [39]. However no crystalline calcium carbonate-type phases were evidenced in our XRD patterns up to 1200°C.

4. Discussion

In the ternary system $Ca(OH)_2$-H_3PO_4-H_2O, there are several known types of calcium phosphate in which the Ca/P molar ratio varies from 0.5 to 2. HA is renowned for its excellent biocompatibility, but its highly crystalline form lack in bioresorbability, and thus requires longer time to create connections with the bone. On the other hand TCP is also well-known as the most widely used bioresorbable material, due to its exceptional compatibility with the living tissues, and to its ability to generate links with the bone without intermediate formation of connective tissue and to promote the rapid regeneration of the surrounding bone. However, the TCP high and unpredictable resorbability rate often leads to high instability *in vivo*. It exists in two crystallographic forms of TCP: β-TCP and α-TCP. The α-form is unstable at low temperatures and it is obtained by heating β-TCP at temperatures above 1120°C [26]. The β-form cannot be obtained directly by precipitation, but it results from the Ca-deficient apatite calcination in the 700–800°C range, by the loss of water. β-TCP form can be also stabilized by doping with small amounts of impurities such as Mg [41].

The temperature effect on bone microstructure and composition was studied by TGA-DSC, SEM-EDS, FTIR and XRD methods. The variability of composition, structure and morphology is essential for understanding the contribution of these factors on bone mass and constitution. In order to control the microstructural, mechanical and compositional characteristics of such materials, to predict and to assess their behaviour depending on the concentration of elements, the understanding of the bone organization is imperative. Organic matrix is a key element for bone strength. Water is the third major constituent of bone, the collagen hydration playing an important role in the bone mechanical properties. Collagen side spaces are different in dry and wet bones. Water can serve as a link between collagen and mineral phases, this link being weakened with high temperature [26,42]. When selecting a proper heat-treatment for producing BCP ceramics with desired compositions (HA/ β-TCP ratios) from bone materials, all these structural features should be taken into full consideration.

The SEM and TGA-DSC techniques helped to characterize the microstructural changes that occur during thermal processing of the bone samples. The SEM analysis method served not only to distinguish inorganic characteristics, but also offered the possibility to identify structural components of cells and micro-morphological details, and to reveal the significant microstructural differences in bone architecture with the heat-treatment temperature. A progressive increase in porosity was found to be induced by increasing the temperature above 800°C (Figure 2-e,f,g). At the cellular level, the micro- and macroporosity, including interconnecting pores, plays a fundamental role in the dissolution and the resorption of the scaffold [43]. Therefore the control of the heat-treatment degradation mechanisms becomes an important objective in obtaining high quality bone substitute materials able to induce the rapid bone regeneration of large osseous defects.

The tailoring of resorbable β-TCP / bioactive HA ratio in the BCP materials might be also dependent on the levels of substitution of other chemical elements present in bone, and how these elements interact with the bone mineral structure during heat-treatment. The EDS analysis did not emphasized significant inorganic chemical composition changes up to 1200°C (except a decrease of C content), but the XRD analysis evidenced some minor structural modification in terms of lattice parameters values, which might be determined by the elemental traces (Na, Mg, Si) incorporation into the HA crystalline lattice. FTIR spectra revealed that with heat-treatment a complete dehydration occurs and collagen gradually degrades up to 800°C. FTIR and XRD analysis showed that the samples' crystallinity increases with the heat-treatment temperature (Figure 4 and 5). A biphasic calcium phosphate type bioceramic (HA+β-TCP) was obtained by performing heat-treatments at temperatures above 800°C. Up to 1200°C, β-TCP transformation in α-TCP was not found. This speaks of the β-TCP phase stability, that can be associated to the presence of Mg in the crystallized bone mineral phase structure (Figure 3), element known to act as a phase stabilizer [41]. A 30% of β-TCP, was induced at 1200°C, for the BCP bioceramic, composition known to posses excellent bone formation capability [16,17,44,45]. The structure of the samples heat-treated at 1200°C is slightly affected (Table 3), the crystalline content being reorganized in a more defined crystalline structure by thermal diffusion. The structural analysis and the thermal behaviour, along with the advantage of the elimination of disease transmitting risks, highlighted the capabilities of our bone thermally derived-materials to be used as biomaterials for bone reconstruction (bone grafts and scaffolds).

5. Conclusions

The correlation of the analysis methods used in this study allowed an understanding of changes produced during the bone heat-treatment up to 1200°C. The temperature played a significant role on the compact bone composition and microstructure. The tailoring of the BCP bioceramic scaffold composition can be controlled by the heat-treatment temperature. A HA:β-TCP concentration of 70:30, considered by many studies as optimal for bone regeneration, has been achieved by annealing the compact bone at 1200°C in argon for 12 hours. No other residual phases had been found.

Acknowledgements

We acknowledge with thanks the financial support of UEFISCDI *PN II-RU 104/2010* project. The authors are grateful to Dr. I. Pasuk for the proof-reading of the manuscript and the helpful discussions.

References

[1] K. Vafai, Porous Media: Applications in Biological Systems and Biotechnology, 1st ed., CRC Press (2010).
[2] B. B. Hole, D. S. Keller, W. M. Burry, J. A. Schwarz, J. Chromatogr. B – Analyt. Technol. Biomed. Life Sci. **879**, 1847 (2011).
[3] S. Guizzardi, M. Raspanti, D. Martini, R. Scandroglio, P. Govoni, A. Ruggeri, Biomaterials **16**, 931 (1995).
[4] V. Benezra, L. W. Hobbs, M. Spector, Biomaterials **23**, 921 (2002).
[5] D. B. Burr, Bone **31**, 8 (2002).
[6] M. Herliansyah, M. Hamdi, A. Ide-Ektessabi, M. Wildan, Mater. Sci. Eng. C – Mater. Biol. Appl. **29**, 1674 (2009).
[7] S. Joschek, B. Nies, R. Krotz, A. Gofpferich, Biomaterials **21**, 1645 (2000).
[8] C. Ooi, M. Hamdi, S. Ramesh, Ceram. Int. **33**, 1171 (2007).
[9] J. R. Lieberman, G. E. Friedlaender, Bone Regeneration and Repair: Biology and Clinical Applications, 1st ed., Humana Press (2005).
[10] C. Laurencin, Y. Khan, S. F. El-Amin, Expert Rev. Med. Devices **3**, 49 (2006).
[11] H. H. G. Handoll, A. C Watts, Cochrane Database Syst Rev. **2**, CD006836 (2008).
[12] C. Seebach, J. Schultheiss, K. Wilhelm, J. Frank, D. Henrich, Injury **41**,731 (2010).
[13] J. H. Rocha, A. F. Lemos, S. Agathopoulos, P. Valério, S. Kannan, F. N. Oktar, J. M. Ferreira, Bone **37**, 850 (2005).
[14] C. V. M. Rodrigues, P. Serricella, A. B. R. Linhares, R. M. Guerdes, R. Borojevic, M. A. Rossi, M. E. L. Duarte, M. Farina, Biomaterials **24**, 4185 (2003).
[15] B. Abdullah, A. H. Shibghatullah, S. S. Hamid, N. S. Omar, A. R. Samsuddin, Cell Tissue Bank. **10**, 205 (2009).
[16] C. Schopper, D. Moser, E. Spassova, W. Goriwoda, G. Lagogiannis, B. Hoering, R. Ewers, H. Redl, J. Biomed. Mater. Res. Part A **85A**, 954 (2008).
[17] F. Ye, X. Lu, B. Lu, J. Wang, Y. Shi, L. Zhang, J. Chen, Y. Li, H. Bu, J. Mater. Sci.-Mater. Med. **18**, 2173 (2007).
[18] S. Ghanaati, M. Barbeck, R. Detsch, U. Deisinger, U. Hilbig, V. Rausch, R. Sader, R. E. Unger, G. Ziegler, C. J. Kirkpatrick, Biomed. Mater. **7**, 015005 (2012).
[19] C. Schopper, F. Ziya-Ghazvini, W. Goriwoda, D. Moser, F. Wanschitz, E. Spassova, G. Lagogiannis, A. Auterith, R. Ewers, J. Biomed. Mater. Res. B – Appl. Biomater. **74B**, 458 (2005).
[20] C. M. Rimnac, A. A. Petko, T. J. Santner, T. W. Wright, J. Biomech. **26**, 219 (1993).
[21] L. F. Lozano, M. A. Peña-Rico, A. Heredia, J. Ocotlán-Flores, A. Gómez-Cortés, R. Velázquez, I. A. Belío, L. Bucio, J. Mater. Sci. **38**, 4777 (2003).
[22] A. Boyde, S. J. Jones, Microsc. Res. Tech. **33**, 92 (1996).
[23] J. I. Catanese, J. D. B. Featherstone, T. M. Keaveny, J. Biomed. Mater. Res. **45**, 327 (1999).
[24] S. Guizzardi, M. Raspanti, D. Martini, R. Scandroglio, P. Govoni, A. Ruggeri, Biomaterials **16**, 931 (1995).
[25] C. Ooi, M. Hamdi, S. Ramesh, Ceram. Int. **33**, 1171 (2007).
[26] D. Tadic, M. Epple, Biomaterials **25**, 987 (2004).
[27] G. E. Fantner, H. Birkedal, J. H. Kindt, T. Hassenkam, J. C. Weaver, J. A. Cutroni, B. L. Bosma, L. Bawazer, M. M. Finch, G. A. Cidade, D. E. Morse, G. D. Stucky, P. K. Hansma, Bone **35**, 1013 (2004).
[28] G-, S.I. Voicu, A.C. Nechifor, S. Garea, Desalination **241**(1-3), 342-348, (2009).
[29] E. M. Raif, M. F. Harmand, Biomaterials **14**, 978 (1993).
[30] C. M. Rimnac, A. A. Petko, T. J. Santner, T. W. Wright, J. Biomech. **26**, 219 (1993).

[31] G. Lazar, K. Zellamaa, I. Vascan, M. Stamate, I. Lazar, I. Rusu, J. Optoelectron. Adv. Mater. **7**, 647 (2005).
[32] G.E. Stan, D.A. Marcov, A.C. Popa, M.A. Husanu, Dig. J. Nanomater. Biostruct. **5**, 705 (2010).
[33] M. C. Chang, J. Tanaka, Biomaterials **23**, 4811 (2002).
[34] G. Socrates, Infrared and Raman Characteristic Group Frequencies—Tables and Charts, John Wiley & Sons Ltd. (2007).
[35] G. E. Stan, I. Pasuk, M. A. Husanu, I. Enculescu, S. Pina, A. F. Lemos, D. U. Tulyaganov, K. El Mabrouk, J. M. F. Ferreira; J. Mater. Sci. - Mater. Med. **22**, 2693 (2011).
[36] M. Markovic, B.O. Fowler, M.S. Tung, J. Res. Natl. Inst. Stand. Technol. **109**, 553 (2004).
[37] J. Neamtu, G. E. Stan, C. Morosanu, C. Ducu, A. Popescu, I. N. Mihailescu, J. Optoelectron. Adv. Mater. **9**, 3821 (2007).
[38] L. Bozec, M. Odlyha, Biophys. J. **101**, 228 (2011).
[39] R. N. Panda, M. F. Hsieh, R.J. Chung, T.S. Chin, J. Phys. Chem. Solids **64**, 193 (2003).
[40] L. Lutterotti, Nucl. Instrum. Methods Phys. Res. Sect. B-Beam Interact. Mater. Atoms **268**, 334 (2010).
[41] D. Lee, P. N. Kumta, Mater. Sci. Eng. C **30**, 1313 (2010).
[42] J. Yan, K. B. Clifton, J. J. Mecholsky, L. A. Gower, J. Biomech. 40, 1641 (2007).
[43] S. J. Hollister, Nat. Mater. **4**, 518 (2005).
[44] Y. Leng, J. Chen, S. Qu, Biomaterials **24**, 2125 (2003).
[45] C. Wang, Y. Duan, B. Markovic, J. Barbara, C. R. Howlett, X. Zhang, H. Zreiqat, Biomaterials **25**, 2507 (2004).